Vibroacoustic testing of panels under a turbulent boundary layer excitation using a space-time spectral synthesis approach

Olivier Robin, Marc Pachebat, Nicolas Totaro, Alain Berry

Vibroacoustic testing of panels under a turbulent boundary layer excitation using a space-time spectral synthesis approach

Olivier Robin, Marc Pachebat, Nicolas Totaro and Alain Berry

Abstract The experimental study of a structure's response to a turbulent boundary layer (TBL) excitation using wind-tunnel or in-vehicle testing generally requires considerable efforts, including the measurement of both turbulent wall-pressure fluctuations and the structure's vibration response. As an alternative method to highly demanding testing procedures and numerical simulations, this paper proposes a computationally efficient method to predict vibroacoustic responses of a panel under a TBL excitation. Space-time realizations of a TBL wall pressure field obtained using a spectral synthesis approach are coupled to a deterministic model so as to predict mean quadratic velocity, and radiated sound pressure and power from a panel under a TBL excitation. Each realization of the wall pressure field and obtained vibroacoustic results can be considered as a virtual experiment. The radiated sound pressure as a function of time can be also obtained, and possibly later used for listening and psychoacoustics studies objectives. A summary of existing experimental and numerical methods for obtaining the vibroacoustic response of panels to a TBL excitation is first presented. The proposed method is then detailed. Results obtained using this method are finally compared to results obtained using controlled laboratory experiments and analytical calculations for a low subsonic flow speed.

Olivier Robin
Groupe d'acoustique de l'université de Sherbrooke, 2500, boulevard de l'université, Sherbrooke, J1K2R1, Canada e-mail: olivier.robin@usherbrooke.ca

Marc Pachebat
LMA CNRS UMR 7031, Ecole Centrale Marseille,
Aix Marseille Univ, F-13402 13453 Marseille Cedex 13 e-mail: pachebat@lma.cnrs-mrs.fr

Nicolas Totaro
Univ Lyon, INSA-Lyon, Laboratoire Vibrations Acoustique, F69621 Villeurbanne, France e-mail: nicolas.totaro@insa-lyon.fr

Alain Berry
Groupe d'acoustique de l'université de Sherbrooke, 2500, boulevard de l'université, Sherbrooke, J1K2R1, Canada e-mail: alain.berry@usherbrooke.ca

1 Introduction

1.1 General problem statement

Vibration of and radiated noise from structures under a turbulent boundary layer (TBL) excitation have been studied for decades with various applications and scales ranging from cars to aircrafts as well as vessels and submarines [1, 2]. It remains a critical research topic that is still looking for accurate and cost-effective simulation and measurement techniques, a major objective being the control of flow-induced noise in a vehicle.

The first documented experimental works concerning TBL-excited panels were conducted in the 1960s [3, 4, 5, 6]. Wind-tunnel investigations were mostly conducted on flat plates of various materials, dimensions and thicknesses, with flow conditions ranging from low-subsonic to high-subsonic flow speeds. The corresponding literature essentially reports wall pressure fluctuations spectra and space-time correlations and vibration spectra of panels and sound power spectra radiated by panels, that correspond to the excitation and the response parts of this vibroacoustic problem, respectively. The measurement of the wall pressure fluctuations (the excitation part) also began in the 1960s [7, 8], this research being still regarded as highly complex in terms of implementation and associated post-processing [9, 10].

Since these pioneering studies, the literature has recorded very few experimental results especially concerning radiated sound power [11, 12, 13, 14]. A great majority of publications report results of numerical calculations that are consequently seldom experimentally validated. Surprisingly, the results of vibroacoustic measurements or calculations are mostly provided in terms of amplitude/frequency representations and using energetic quantities (mean squared velocity, sound power or ratios like sound transmission loss). These quantities are sometimes averaged as a function of frequency (practically, in octave bands or fractional octave bands such as a third or a twelfth of an octave), or even expressed in terms of a single overall level. This provides compact data representations that are certainly useful but nevertheless opposite to a detailed analysis including human perception. As pointed out by Oettle *et al.* [15],

> The human brain is not only sensitive towards the level of steady broadband noise, but distinctive features such as tonality or modulation draw the attention of the vehicle occupant and impact negatively on perception. (...) A key to achieving future vehicle refinement is bringing together an understanding of unsteady onset flow conditions, their impact on cabin sound pressure level and modulation and, in turn, the impact of noise level and modulation on psychoacoustic perception.

Among the keypoints that are currently missing towards a better understanding and comprehension of TBL-induced problems, two can be highlighted :

- The measurement of both wall-pressure fluctuations and structure's response using wind-tunnel or in-vehicle testing generally require considerable efforts, with associated data that nevertheless show large scatter. A reduced number of experiments is thus conducted and then available for validating the results of

numerical computations. Alternative methods to highly demanding testing or simulation procedures are thus needed.
- The perception of the radiated sound from TBL-excited structures as a function of time is hardly considered even if it should be a primary goal. This is especially true for transportation applications for which flow conditions are usually slightly unsteady and lead to fluctuations of level and frequency content as a function of time.

1.2 Alternative experimental methods to conventional wind-tunnel testing

Several strategies have been proposed to reduce technical constraints and increase the precision of measurements related to TBL-induced problems. The standardized method using coupled rooms for testing the transmission loss of panels under a diffuse acoustic field (DAF) excitation has been occasionally used as an alternative measurement, but is known to be not representative of a TBL excitation.

Compared with the generation of a DAF that only involves acoustic components, the specific case of a TBL means reproducing acoustic and convective components, the latter having smaller spatial scales than the acoustic scale for subsonic flows. The wall-pressure fluctuations induced by a TBL surface pressure are indeed a superposition of hydrodynamic and acoustic pressures whose levels differ by several orders of magnitude [16]. In addition to level difference, a keypoint in TBL-related vibroacoustics problems lies in the introduction of other dimensions than the classical acoustic wavelength λ_0 and the structural wavelength λ_s, that is the convective wavelength λ_c. Let's consider a low speed flow (for example, a Mach number of 0.1). The convective velocity U_c is a fraction of the free flow velocity U_∞ (usually taken as $U_c \approx 0.6 - 0.7U_\infty$). The ratio between acoustic and convective scales thus reaches a value of approximately ten and for a speed of sound of 340 m/s and at a frequency of 1000 Hz, the acoustic wavelength equals 34 cm, while the convective wavelength will be approximately 2.4 cm ($= 340 \times 0.1 \times 0.7/1000$). Due to the large range of scales and levels, the simultaneous measurement and/or generation of both acoustic and convective components is an experimental challenge.

Several approaches relying on sound synthesis has been considered so as to recreate an actual TBL excitation using loudspeaker arrays. Kirkeby and Nelson[19] were the first to propose the generation of plane sound waves. Several researchers extended this approach to the reproduction of random pressure fields such as Bravo and Maury [17, 20, 21, 18] who obtained theoretical and experimental results concerning the reproduction of a DAF- and a TBL-induced wall pressure field using a near-field array of loudspeakers and a least squares method to define the complex signal to be fed to each reproduction source. Nevertheless, in the case of the TBL, the reproduction of its statistics was only feasible at low frequency due to the rapid decay of the TBL streamwise and especially spanwise correlation lengths with frequency. Bravo and Maury suggested that the synthesis of the TBL-induced panel

vibroacoustic response could be a more viable strategy, since focusing on the panel response helps to significantly reduce the number of reproduction sources required.

Another approach based on the concept of uncorrelated plane waves, a least squares approach and a synthetic source array was proposed by Aucejo *et al.* [22]. The synthetic array principle allows simulating the effect of an array of acoustic sources from sequential measurements using a single source. This allows a higher flexibility of the experimental set-up regarding the total number of monopoles required to suitably reconstruct wall pressure statistics, compared with the work of Bravo and Maury [20, 21]. The results obtained on an academic structure, a clamped panel, showed that the structural velocity autospectral density function of the panel subjected to TBL excitation could be effectively reproduced.

Robin *et al.* [23] used three different approaches to define the reproduction sources complex amplitudes (a least squares based approach, a Wave Field Synthesis based approach and the a Planar Nearfield Acoustic Holography based approach), that were then coupled to the synthetic source array concept introduced by Aucejo *et al.* [22]. Experimental results were obtained for a simply supported panel, that confirmed that even with a synthetic source array approach, the technical constraints for the reproduction of a TBL excitation were still dictated by the acoustic wavelength and the convective wavelength (the smallest wavelength to be reproduced for a subsonic excitation). It was also confirmed that the exact reproduction of the TBL wall pressure fluctuations was not fundamental for the reproduction of the TBL-induced panel response, as suggested by Bravo and Maury [21, 20]. Recently, Merlo *et al.* [24] investigated the control of loudspeaker arrays via their acoustic radiation modes (ARM) to replace complex and costly flight and wind-tunnel measurements, but no example of TBL reproduction was yet provided in this work. Pasqual [25] suggested on his side using the ARM of a spherical array to reproduce complex sound fields. In summary, the proposed methods are generally not able to accurately and directly reproduce the most energetic components of a subsonic TBL that are located outside the acoustic wavenumber domain

Marchetto *et al.* [26] suggested another approach to experimentally predict the vibration response of panels under a TBL excitation, by explicitly separating the forcing wall-pressure fluctuations from the vibration behavior of the panel. In this work, the idea of an *ex situ* characterization of a panel's response under TBL excitation is suggested and validated : once the excitation is characterized, the response of a panel under the considered excitation can be deduced, making the experimental facility no longer needed.

A last possibility to alleviate some constraints linked to wind-tunnel testing relies in the similitude concept, a main application field of this concept being surely aerodynamics with tests on a scale-model aircraft to define the aerodynamic characteristics of a full-scale aircraft [27]. The similitude concept has been also widely applied in structural engineering, see a review in [28]. Recent works related to vibroacoustics have especially aimed at defining scaling laws for predicting the vibration response of a structure using a scaled model in a wind tunnel. In this case, structural parameters as well as flow parameters must be properly scaled. Vibration measurements on a simplified cylindrical structure in wind-tunnel were put in similitude between a

scaled model and a full-scale model [29] . In [30], both vibration auto-spectral and cross-spectral density functions, previously measured in a wind-tunnel facility on a set of three plates, were successfully scaled which opens the possibly of scaling the radiated sound pressure under a TBL excitation.

1.3 Numerical methods for the prediction of the vibroacoustic response of panels

Two main strategies are generally considered for predicting the vibro-acoustic response of structures excited by surface pressure fluctuations. The first one relies on computational fluid dynamics (CFD) and computational aeroacoustics (CAA) to solve external flow problems. Incompressible large eddy or detached eddy simulations are used to compute the surface pressure fluctuations for vehicles or simplified structures, that are then coupled to finite element method or statistical energy analysis approaches for interior noise simulation [31]. CFA or CAA simulations are nevertheless highly demanding, and usually require intense parallel computing. So as to relax computational constraints that are important for such simulations, reduced-order modeling methods like the dynamic mode decomposition and the proper orthogonal decomposition are usually employed to better describe the wall pressure excitation on a structure [15]. As an example, Druault *et al.* [32] proposed an application of the proper orthogonal decomposition to characterize and separate of both acoustic and turbulent components of the wall pressure excitation, that was tested from wall pressure fields synthesized from theoretical averaged models or obtained from lattice Boltzmann method simulations. Hu *et al.* tested the use of synthetic turbulence generated by the fast random particle–mesh method to simulate flat plate turbulent boundary layers under zero pressure gradient [33], and wall-pressure fluctuations on an Airbus-A320 fuselage in flight conditions [9].

The other approach that is used in many numerical approaches in order to predict vibrational responses of structures excited by turbulent flow couples the cross-spectral density function describing the wall pressure fluctuations to a deterministic vibroacoustic model (generally defined through the use of finite element modeling). Since a very large number of distributed points on the surface of the structure needs to be considered according to theory, usual requirements in terms of ideal mesh size are deemed unrealistic in many practical cases and many works aim at reducing the computational cost of such approaches. Modeling techniques considered as hybrid approaches which combine statistical and deterministic methods were investigated in [34] so as to relax meshing constraints. In order to implement a numerical synthesis of aeroacoustic wall-pressure field, Hekmati *et al.* [35] proposed a method based on the Cholesky decomposition of analytical expressions of the cross power spectral density of a DAF and a TBL (defined using the Corcos's model, [7]). Recently, Karimi *et al.* [36, 37] combined the uncorrelated wall plane wave (UWPW) technique [38] with a finite element method. The cross spectrum density function of the wall pressure field was defined either by empirical models from literature or

from experimental data. The response of a structure subject to a TBL excitation was then obtained from an ensemble average of the different realizations of the UWPW and the technique was shown to be computationally efficient as it rapidly converged using a small number of realizations. Predicted velocity spectra compared well with measured velocity spectra in two different anechoic wind tunnels and on two different panels.

In [39], it was proposed to couple a space-time synthesis approach (*i.e.* several consecutive realizations of a wall pressure field) to a deterministic model so as to predict sound transmission loss of and radiated sound pressure from panels under a DAF excitation. Both quantities were efficiently predicted and good agreement was obtained with measurements and finite element method predictions. The formalism is similar to the UWPW technique [38], but the applied probability density functions (PDF) can be varied (*i.e.* can be defined as Gaussian, or not). This can not be achieved with the UWPW technique, for which the normalized sum of plane waves that is used will tend toward a Gaussian distribution according to the central limit theorem.

This space-time, 2D+t, synthesis approach is here extended to the case of TBL-excited panels. Besides an additional flexibility gained compared with the UWPW technique in terms of PDF definition, the proposed 2D+t method has several advantages, that can provide adequate solutions to the keypoints previously expressed in section 1.1 : (1) Each realization of the wall pressure field and obtained vibroacoustic results can be considered as a virtual experiment, or a series of them can mimic an experiment of variable length, and (2) The radiated sound pressure as a function of time and under a random excitation (DAF-TBL) can be obtained and used for listening purposes.

This chapter first describes the suggested calculation process. Measurements made on a rectangular aluminum panel with controlled simply-supported boundary conditions and tested in a low-speed anechoic wind-tunnel at a flow sped of 40 m/s [40] are used as a test case for extending the approach to the case of a TBL excitation.

2 Spectral synthesis of the wall pressure field induced by a TBL

In the proposed method, each particular realization of a turbulent pressure (random draw) corresponds to an induced flexural response as well as a radiated pressure field. Among the difficulties encountered, the three physical scales of the problem (convective, structural and acoustic) cover very different intervals. As indicated in the introduction part, the experimental methods that intend to mimic vibroacoustic tests in wind tunnel have difficulty to describe wave numbers associated with subsonic convective phenomena [20, 22], while inversely numerical methods in fluid mechanics require huge efforts for correctly simulating the acoustic waves generated by the flow [44].

In this context, a representation of the turbulent pressure by the realization of a random process allows on the one hand, to integrate in the synthesis process the relevant physical information for all scales, and on the other hand, to solve a direct formulation of the vibroacoustic problem giving access in a simple way to the time radiated pressure.

In the hypothesis of a homogeneous and stationary flow, the synthesis by Cholesky decomposition of the cross-correlation matrix [45, 35] is replaced by a spectral synthesis [43, 42] which largely reduces the computational effort. This is achieved by inverse fast Fourier transform (FFT) of a physical model in the wavenumber-frequency domain. Thanks to the FFT algorithm efficiency, the generation of turbulent wall pressure field in the physical domain (x, y, t) is very fast compared to other approaches.

Fluid Density	ρ (kg.m^{-3})	1.20
Sound velocity	c_0 (m.s^{-1})	343
Dynamic viscosity	ν (m^2.s^{-2})	$15.1\,10^{-6}$
Free stream velocity	U_∞ (m.s^{-1})	40
Convection velocity	$U_c = 0.6\,U_\infty$ (m.s^{-1})	24

Table 1 Physical characteristics of the considered Turbulent Boundary Layer.

2.1 Space time spectral synthesis (2D+t)

In this work, a low speed subsonic Mach number flow ($M_\infty = 0.12$) is considered to generate a homogeneous and stationary turbulent boundary layer with no pressure gradient over a smooth rigid wall (see tables 1 and 2). The flow is assumed to be both homogeneous (in space) and stationary (in time). As a consequence, a sample of a pressure field over the spatio-temporal domain $L_x \times L_y \times T$ can be generated as a draw of a stochastic process using a spectral synthesis method, as explained in the following.

Let $p(x, y, t)$ denote the fluctuating boundary pressure over a rigid wall in the (Oxy) plane: we propose to simulate $p(x, y, t)$ as a random Gaussian field with zero-mean even though observations of $p(x, y, t)$ beneath a TBL exhibit slightly non

Streamwise length	L_{px} (m)	0.600
Spanwise width	L_{py} (m)	0.525
Young modulus	E_p (Pa)	$70.\,10^9$
Density	ρ_p (kg.m^{-3})	2700
Poisson ratio	ν_p	0.3
Thickness	h_p (mm)	2.4

Table 2 Physical characteristics of the panel

Gaussian statistics, see e.g. Schewe [47]. The main interest is that the prescription of its correlation function, or equivalently its Fourier spectrum, completely specifies a Gaussian process. Then the space-time correlation function $R =< p(x,y,t)p(x+\xi_x, y+\xi_y, t+\tau) >$ (<> denotes an ensemble average, and $\xi_{x,y}$ are the separations between two points in x and y directions, respectively) of an homogeneous and stationary process $p(x,y,t)$ reduces to $R(\xi_x,\xi_y,\tau)$. It can equivalently be described by its 2D+t Fourier transform $P(k_x,k_y,\omega)$ called the wavenumber-frequency power spectrum.

$N_x \times N_y \times N_t = 256 \times 256 \times 2048$			
Δx	0.0028 m	k_x^{max}	1108.3 rad.m^{-1}
Δy	0.0025 m	k_y^{max}	1266.7 rad.m^{-1}
Δt	$4.883\,10^{-4}$s	f^{max}	1023 Hz
L_x	0.72 m	Δk_x	8.727 rad.m^{-1}
L_y	0.63 m	Δk_y	9.973 rad.m^{-1}
T	1 s	Δf	1.0 Hz

Table 3 ($N_x \times N_y \times N_z$): numerical size of the simulated wall pressure; ($\Delta x, \Delta y, \Delta t$): corresponding time and space resolution; (Δk_x, Δk_y, Δf): wavenumber and frequency steps; (L_x,L_y,T) and ($\pm k_x^{max}$,$\pm k_y^{max}$,$\pm f^{max}$): intervals covered by the simulated wall pressure in physical and Fourier domain respectively.

In this case, the simulation of a wall pressure field according to a spectral model sums up to a simple and fast spectral synthesis algorithm which permits to generate draws of a stationary Gaussian process. The principle of this method is to filter a Gaussian white noise using the targeted spectrum. In practice, one first draws a discrete set of $N_x \times N_y \times N_t$ independently and identically distributed Gaussian real random variables g_{lmn} with zero mean, thanks to a pseudo-random number generator. The discrete indices (l,m,n) correspond to continuous variables (x,y,t). Then the 3D Discrete Fourier Transform of g_{lmn} denoted by $G_{l'm'n'}$ is a set of $N_x \times N_y \times N_t$ identically distributed Gaussian complex random variables [43]. By construction $G_{l'm'n'}$ obeys the Hermitian symmetry of the Fourier transform of real signals (where discrete indices (l',m',n') correspond to continuous variables (k_x,k_y,ω)).

In a discrete representation, the relationship between the space-time correlation R_{lmn} and the wavenumber-frequency power spectrum $P_{l'm'n'}$ is given by the following 3D discrete Fourier transform:

$$P_{l'm'n'} = \sum_{l=0}^{N_x-1} \sum_{m=0}^{N_y-1} \sum_{n=0}^{N_t-1} R_{lmn}.e^{2\mathrm{j}\pi\left(\frac{n.n'}{N_t}-\frac{l.l'}{N_x}-\frac{m.m'}{N_y}\right)}, \quad (1)$$

where $N_x \times N_y \times N_t$ is the numerical size of the domain in space and time.

The physical domain is defined by (L_x, L_y, T) where T is the duration of the simulation. The dimensions $L_x \times L_y$ of the simulated wall pressure are chosen to be slightly greater than the size of the panel : $L_x/L_{px} = 1.2$ and $L_y/L_{py} = 1.2$.

The physical domain is sampled by $N_x \times N_y \times N_t$ points (see Table 3):

$$\begin{cases} N_x = k_x^{max} L_x/\pi & = 2\pi(\Delta x \Delta k_x)^{-1}, \\ N_y = k_x^{max} L_y/\pi & = 2\pi(\Delta y \Delta k_y)^{-1}, \\ N_t = 2f^{max} T & = (\Delta t \Delta f)^{-1}. \end{cases} \tag{2}$$

Following the 1D algorithm from Davies [42] and formally applying it to space-time (2D+t) case, the pressure field p_{lmn} is given by the inverse discrete Fourier transform of the product $\sqrt{P}.G$ where P is a given discrete wavenumber-frequency power spectrum $P_{l'm'n'}$ (the targeted physical model), and G is a draw of $N_x \times N_y \times N_t$ identically distributed Gaussian complex random variables with Hermitian (transconjugate) symmetry:

$$p_{lmn} = \sum_{l'=0}^{N_x-1} \sum_{m'=0}^{N_y-1} \sum_{n'=0}^{N_t-1} \frac{\sqrt{P_{l'm'n'}}\, G_{l'm'n'}}{N_x N_y N_t} e^{-2\mathrm{j}\pi\left(\frac{n.n'}{N_t} - \frac{l.l'}{N_x} - \frac{m.m'}{N_y}\right)}. \tag{3}$$

In practice, G is obtained from the 3D Fourier transform of $(N_x \times N_y \times N_t)$ pseudo-random real values drawn from the Gaussian distribution, to ensure the Hermitian symmetry of G.

The resulting 2D+t discrete pressure field p_{lmn} is a sample of a real valued spatio-temporal process; it is Gaussian, and has zero mean as soon as $P_{000} = 0$. The wavenumber-frequency power spectrum of p_{lmn} is imposed by $P_{l'm'n'}$.

In order to avoid aliasing artifacts, the size of the synthesis $(N_x \times N_y \times N_t)$ is adapted to cover the domain where the energy in $P_{l'm'n'}$ is present. This depends upon the flow parameters and physical model used.

On Fig.1, the simulated pressure obtained from the spectral synthesis is shown for three neighbouring instants. As in a turbulent field, it exhibits a superposition of a large number of spatial scales that are convected along the streamwise axis Ox. The spectral synthesis and the statistical properties of the pressure field shown on Fig.1 are detailed in the next section.

2.2 Validation of the synthesized wall pressure statistics

The statistical properties of the wall pressure are chosen here according to the Mellen model [46]:

$$P(k_x, k_y, \omega) = S_{pp}(\omega) \frac{2\pi(\alpha\beta k_c^2)^2}{[(\alpha\beta k_c^2)^2 + (\beta k_c k_y)^2 + (\beta k_c)^2.(k_c - k_x)^2)]^{3/2}}, \tag{4}$$

where the streamwise and spanwise correlation length are fixed to $\alpha = 0.12$ and $\beta = 0.7$. The convective wavenumber is $k_c = \omega/U_c$ (rad.m^{-1}) where the value of the convection velocity $U_c = 0.6\, U_\infty$ is fixed for each frequency.

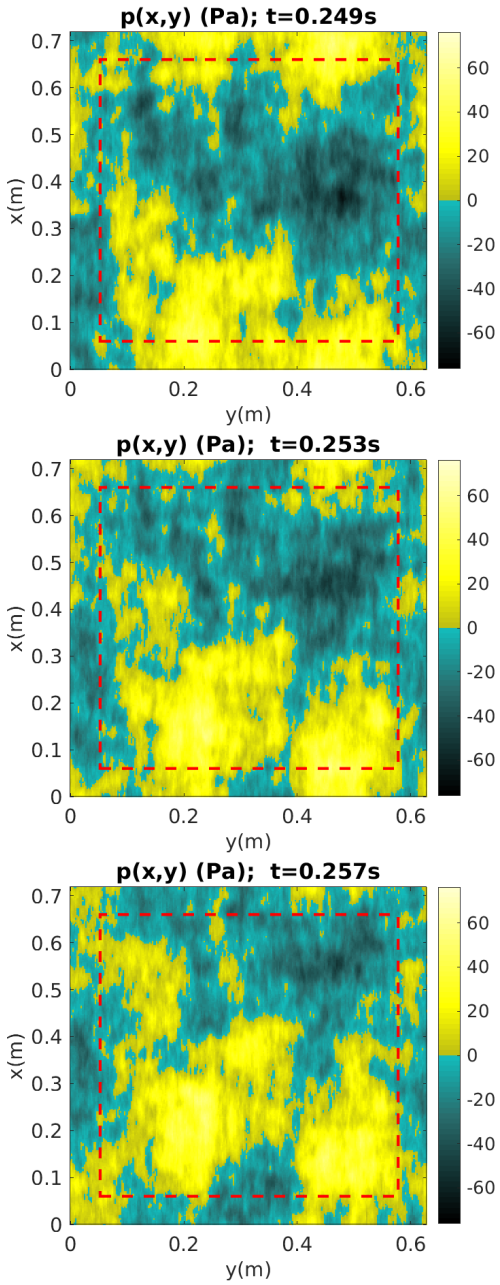

Fig. 1 Three snapshots separated by $\Delta t = 4.10^{-3}\,s$, of the time pressure simulated over the flat surface. The time step is chosen to highlight the streamwise convection of the fluctuations, along the vertical axis and oriented as Ox. The red dash line indicates the physical size of the considered panel. The instantaneous pressure amplitude in Pascals is given by the color bar.

In Eq. (4), the spectrum of the pressure $S_{pp}(\omega)$ [Pa]^2 must be specified before the spectral synthesis. To that aim, the measured autospectral density (in red on fig. 2) is filtered at high frequency, extended towards low frequencies, and interpolated according to the frequency resolution of the desired simulation (see Table 3). The result is shown in blue solid line on Fig. 2 and is used to specify the spectrum of the pressure $S_{pp}(\omega)$ in Eq. (4).

The wavenumber-frequency spectrum, Eq. (4), is then introduced into Eq. (3) to obtain one draw of p_{lmn} that represents one realization of the simulated wall pressure field $p(x, y, t)$.

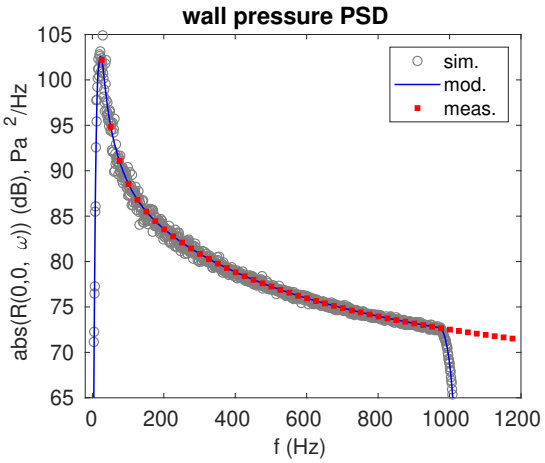

Fig. 2 Power Spectrum Density of the wall (point) pressure : measured (red square see section 4), interpolated from measurements (blue line), estimated (grey circles) from the simulated wall pressure and averaged over the panel area.

In order to check the statistical properties of the simulated wall pressure from the spectral synthesis (Eq. (3)), the wavenumber-frequency spectrum can be estimated, and defined as :

$$\hat{P}(k_x, k_x, \omega) = \frac{1}{N} \sum_{1}^{N} \left[\lim_{L_x, L_y, T \to \infty} \frac{1}{L_x L_y T} \frac{\hat{p}(k_x k_y, \omega) \hat{p}^*(k_x k_y, \omega)}{\Delta k_x \Delta k_y \Delta f} \right], \tag{5}$$

where $\hat{p}(k_x k_y, \omega)$ is the Fourier transform of $p(x, y, t)$, $\hat{p}^*$ is its complex conjugate, and N the number of averaging used for the estimation. Using the inverse Fourier transform of $\hat{P}(k_x, k_x, \omega)$ over (k_x, k_y) and then ω, we can obtain respectively the frequency cross-correlation $R(\xi_x, \xi_y, \omega)$, and the broad-band space cross-correlation $r(\xi_x, \xi_y, \tau)$ where ξ_x, ξ_y and τ denote separations along Ox, Oy and time axis.

In practice, since we are using here a single discrete realization of p_{lmn}, the estimator used to compare $\hat{P}(k_x, k_x, \omega)$ of Eq. (5) and $P(k_x, k_y, \omega)$ of Eq. (4) is reduced to:

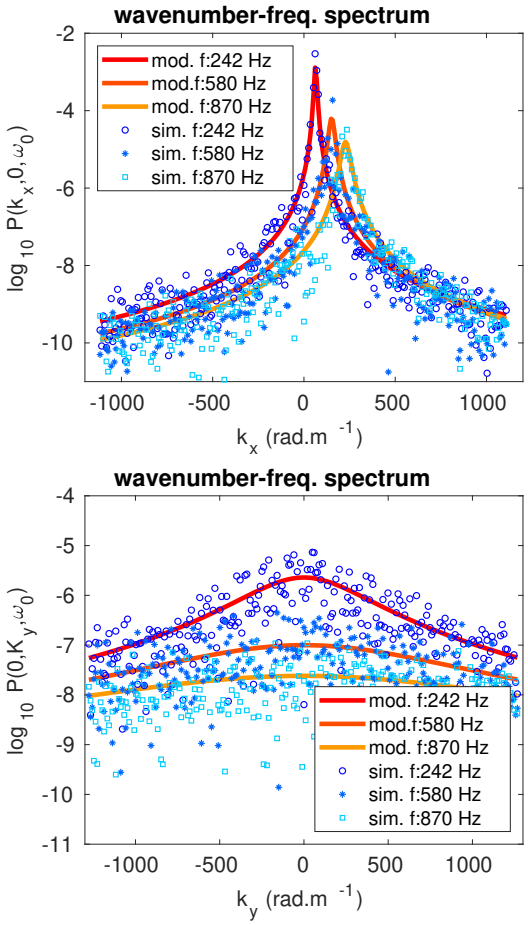

Fig. 3 Wavenumber-frequency spectrum $P(k_x, k_y, \omega)$ at three chosen frequencies. Bottom: spanwise $P(0, k_y, \omega_0)$. Top: streanwise $P(k_x, 0, \omega_0)$: the peak corresponding to the convective ridge appears at $k_x = 2\pi f/U_c$ rad.m^{-1}. Solid curves : Mellen model (Eq. (4)). Symbols : estimation from one draw of the simulated wall pressure (Eq. (6)).

$$\hat{P}_{l'm'n'} = \frac{1}{L_x L_y T} \frac{p_{l'm'n'} p^*_{l'm'n'}}{\Delta k_x \Delta k_y \Delta f}, \tag{6}$$

where $p_{l'm'n'}$ is the 3D discrete Fourier transform of p_{lmn}.

The frequency cross-correlation $R(\xi_x, \xi_y, \omega)$ of the simulated field is obtained after a 2D inverse Fourier transform of $\hat{P}_{l'm'n'}$ (Eq. (6)). The result noted $R_{lmn'}$ is represented in PSD units for zero-space separation $R(0, 0, \omega)$ on Fig. 2 (grey circles). It corresponds to the point pressure spectrum averaged over the $(N_x \times N_y)$ spatial points and exhibits a good statistical convergence towards the PSD interpolated from the measurements (blue line).

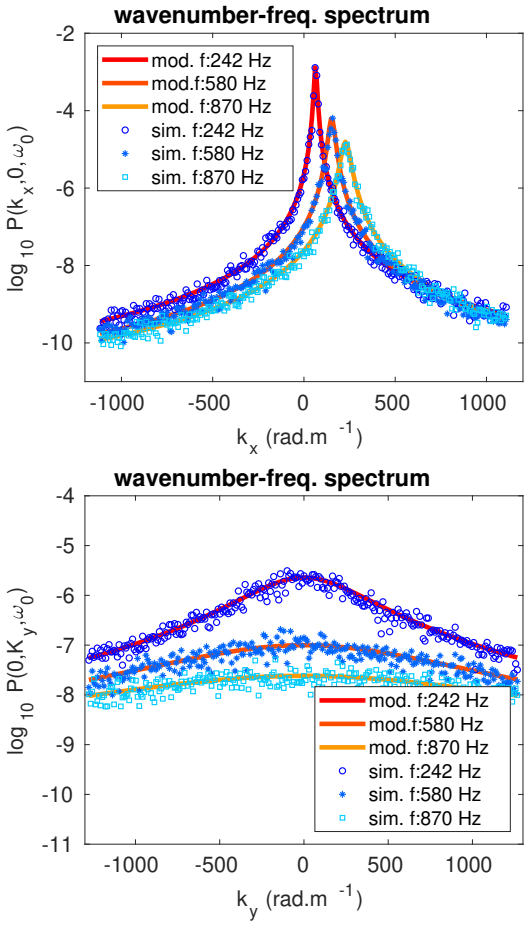

Fig. 4 Wavenumber-frequency spectrum $P(k_x, k_y, \omega)$ at three chosen frequencies. Bottom: spanwise $P(0, k_y, \omega_0)$. Top: streanwise $P(k_x, 0, \omega_0)$: the peak corresponding to the convective ridge appears at $k_x = 2\pi f/U_c$ rad.m^{-1}. Solid curves : Mellen model (Eq. (4)). Symbols : estimation from 10 realizations of the simulated wall pressure (Eq. (5) with $N = 10$).

Figure 2 shows that the simulated space-time pressure field p_{lmn} exhibits a point spectrum that statistically converges towards $S_{pp}(\omega)$ chosen in Eq. (4).

In order to check the simulated space-time pressure field p_{lmn} in the wavenumber domain, the wavenumber-frequency spectrum $\hat{P}_{l'm'n'}$ from Eq. (6) is plotted on Fig. 3 (symbols) and compared to the Mellen model of Eq. (4) (solid lines). Three particular frequencies are chosen for the streamwise (top) and spanwise (bottom) plots. Since Eq. (6) is estimated on a single realization (no ensemble averaging), the resulting standard deviation is high. But exactly like experimenters do, one can verify that an averaging over N realizations of the simulated pressure using Eq. (5), reduces the

standard deviations and shows a statistical convergence of $\hat{P}_{l'm'n'}$ towards the Mellen model of Eq. (4), as shown on Fig. 4 whith $N = 10$.

The space-time wall pressure obtained with the spectral synthesis of Eq.(3) is now checked to be statistically compliant with the targeted properties, and can be used in the following as an excitation term for a flat baffle panel.

3 Coupling wall pressure statistics to a model of a structure

The acoustic radiation of the plate excited by the synthesized wall pressure field is computed in a two-steps process: the acoustic field is obtained from the velocity field of the plate computed in a preliminary step. It is thus assumed that:

- the fluid is light enough to be neglected when computing the velocity response of the plate.
- the vibration of the plate does not affect the wall pressure field.

3.1 Vibration response of the panel

The panel under study is a simply supported rectangular thin plate of dimensions $L_{Px} \times L_{Py}$ and of thickness h_P. It is made of a homogeneous isotropic material having a Young's modulus E_P, a density ρ_P and a Poisson's ratio ν_P. In this configuration, natural angular frequencies ω_{rs} and mode shapes $\phi_{rs}(x, y)$ of the panel are respectively given by Eq. ((7)) and Eq. ((8)):

$$\omega_{rs} = \sqrt{\frac{D}{M}} \left(\left(\frac{r\pi}{L_{Px}} \right)^2 + \left(\frac{s\pi}{L_{Py}} \right)^2 \right), \tag{7}$$

$$\phi_{pq}(x, y) = sin\left(\frac{r\pi}{L_{Px}} x \right) sin\left(\frac{s\pi}{L_{Py}} y \right). \tag{8}$$

The vibrational velocity of the panel can be expressed as a sum of contributions of mode shapes as

$$V(x, y, \omega) = \sum_{r=1}^{\infty} \sum_{s=1}^{\infty} \frac{\mathrm{j}\omega F_{rs}(\omega)\phi_{rs}(x, y)}{M_{rs}\left(\omega_{rs}^2 - \omega^2 + \mathrm{j}\eta\omega\omega_{rs}\right)}, \tag{9}$$

where $M_{pq} = \rho_P h_P \frac{L_{Px} L_{Py}}{4}$ is the modal mass, ω is the excitation angular frequency and η is the damping loss factor (considered constant as a function of frequency). The modal force $F_{rs}(\omega)$ is defined as:

$$F_{rs}(\omega) = \int_0^{L_{Px}} \int_0^{L_{Py}} \tilde{p}_{lmn}(x, y, \omega)\phi_{rs}(x, y)\, \mathrm{d}x\, \mathrm{d}y, \tag{10}$$

where $\tilde{p}_{lmn}(x, y, \omega)$ is the Fourier transform of $p_{lmn}(x, y, t)$. All the information coming from the pressure field is condensed in only one complex value per mode at each frequency. To not lose any information, Eq. ((10)) is discretized using the grid mesh of the pressure field as listed in Tab. 3. Finally, the spatially averaged mean square velocity $\langle V^2 \rangle$ of the plate is calculated as :

$$\left\langle V^2(M,\omega) \right\rangle_{S_P} = \frac{1}{S_P} \int_{S_P} V(M,\omega) V^*(M,\omega) \, \mathrm{d}S_P. \tag{11}$$

3.2 Acoustic response of the panel

In case of a flat baffled panel, the radiated pressure can be computed using the Rayleigh's integral:

$$P(M_0,\omega) = \int_{S_P} \mathrm{j}\omega\rho_0 V(M,\omega) G(M_0, M, \omega) \, \mathrm{d}S_P, \tag{12}$$

where M is a point of coordinates $(x, y, 0)$ on the surface of the plate and M_0 is a listening point of coordinates (x_0, y_0, z_0). The Green's function $G(M_0, M, \omega)$ is

$$G(M_0, M, \omega) = \frac{1}{2\pi} \frac{e^{-\mathrm{j}kR}}{R}, \tag{13}$$

with $R = \sqrt{(x - x_0)^2 + (y - y_0)^2 + z_0^2}$. The radiated sound power from the plate can be expressed as a function of plate velocity $V(M, \omega)$ and of pressure radiated on the surface of the plate $P(M_0, \omega)$

$$\Pi^{\mathrm{rad}}(\omega) = \frac{1}{2} \int_{S_P} \Re \left(P(M,\omega) V^*(M,\omega) \right) \, \mathrm{d}S_P \tag{14}$$

where $\Re(\bullet)$ and $\bullet^*$ stand respectively for the real part and the complex conjugate of $\bullet$.

4 Experimental methods

4.1 Description and setup of the structure under test

The considered TBL excitation in this study was obtained in a low-speed anechoic wind tunnel at Université de Sherbrooke, and is considered to be a zero-pressure-gradient TBL developing over a flat plate with a free-flow velocity of 40 m/s. The panel under study had controlled simply-supported boundary conditions along its four edges obtained using a dedicated procedure and setup [48]. The geometrical

and mechanical properties of the panel are reported in Table 2. A value of 0.95 % for the average structural loss factor was determined following the -3dB method on the ten first vibration modes.

A 1.22 x 2.44 m^2 rigid panel made of medium density fiberboard (0.019 m thickness) was mounted in the anechoic wind tunnel at the end of the convergent (see Fig. 5(a,b)). In order to help the TBL excitation develop, a sandpaper strip was glued at the intersection of the convergent and of the panel so as to prevent any discontinuity between the convergent and the baffle. The panel was installed into the baffle and was positioned on its own supporting stand (see Fig. 5(c)), and thus no mechanical link exists between the panel and the baffle.

The measurement space below the panel under test was acoustically treated using rigid ceiling tiles and backed by panels of compressed 1-in thick glass wool. Sound absorbing material was placed on the panel's stand so as to limit sound reflections, and even if the floor of the measurement space opens towards the anechoic room, it was covered will compressed glass wool panels.

4.2 Wall pressure fluctuations characteristics

In [26], a precise characterization of the flow was conducted in the same wind tunnel with a strictly similar setup (i.e. identical position from the wind-tunnel convergent, same flow speed and environmental conditions). The wall-pressure fluctuations of the turbulent flow generated over the baffle were measured with a flush-mounted microphone array [49]. The decay rates and the convection velocity were extracted as a function of frequency from these measurements (the Mellen model [46] was fitted to the measured WPF using the least square method). At the exception of the convection velocity that was considered constant as a function of frequency, the frequency-dependent results of this identification (decay rates, autospectral density), were used for all the calculations made using the proposed spectral synthesis approach.

4.3 Measurement of vibration of and radiated sound pressure and sound power from the panel

Vibration measurements were made using a set of five mono-axis low weight accelerometers so as to limit the added mass (approximately 15 g total added mass per measurement, including cables). Four sets of five measurements points were used and the average quadratic velocity was finally calculated using 20 discrete measurement points.

The radiated sound power was estimated using a 48-microphone array placed along a parallelepipedic measurement surface following ISO3744 standard [50], see Fig. 5(c). The calculation of sound pressure level averaged over the measurement surface and sound power level were made according to ISO3744 standard. Concern-

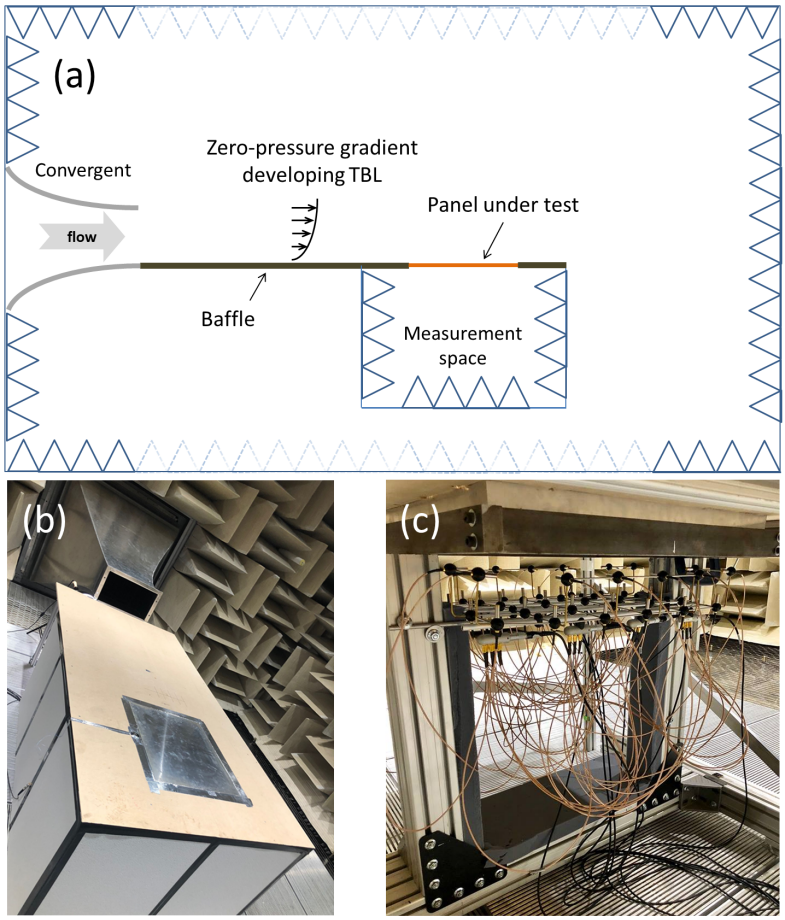

Fig. 5 (a) Schematic description of the experimental setup – (b) Picture of the panel installed in the anechoic wind-tunnel - (c) Picture of the panel on its own stand, including the microphone array.

ing sound pressure comparison with results obtained using the proposed approach, a single microphone from the array was considered.

5 Results

5.1 Mean quadratic velocity

In the upper part of Fig. 6 is presented a comparison between analytical calculations (Eq. (11)) and experimental results for the mean quadratic velocity. It can be seen that numerical results are in excellent agreement with analytical results.

The middle part of Fig. 6 shows five different results, that were obtained using the proposed procedure and five different realizations of the simulated WPF using Eq. (5). These can be considered as five different virtual experiments results (tests under different realizations of the same excitation), and are superimposed to previous analytical and experimental results. The agreement between these virtual experiments and analytical and experimental results is overall very satisfactory.

The lower part of Fig. 6 shows the same results on a reduced frequency range (100-300 Hz), illustrating the results of the different draws of the WPF. Each virtual experiment lead to a result that is distributed around the smooth analytical result. The mean quadratic velocity value at peaks varies with the considered draw, showing that the procedure leads to variations in terms of coupling between the wall-pressure field and the panel.

5.2 Radiated sound power

In the upper part of Fig. 7 is presented a comparison between analytical calculations (Eq. (14)) and experimental results for the radiated sound power. As for the mean quadratic velocity, the agreement between analytical and measured mean quadratic velocity is very satisfactory.

The middle part of Fig. 7 shows five different results, that were obtained using the proposed procedure and three different realizations of the simulated WPF using Eq. (5). As for the mean quadratic velocity, the agreement between these virtual experiments and analytical and experimental results is overall very satisfactory, despite a level difference that rises with increasing frequency.

The lower part of Fig. 6 shows the same results on a reduced frequency range (now from 20 to 200 Hz). It appears that the sound power level, especially at peaks, is a function of the considered draw (with a mean that will tend to the analytical result) showing that the approach can mimic a series of short-time experiments.

5.3 Radiated sound pressure

Successive draws can be also used to construct a short-time Fourier transform representation of the radiated sound pressure (spectrum as a function of time), and then

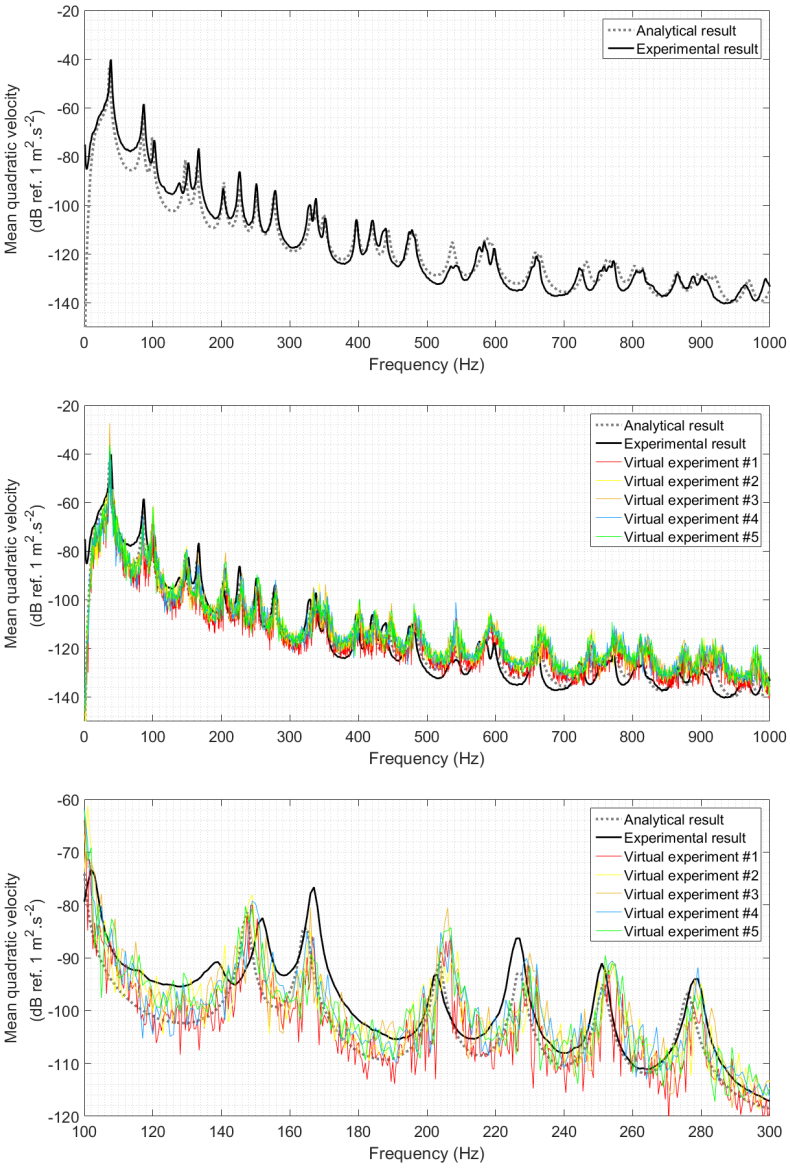

Fig. 6 (Upper part) Analytical calculations (Eq. (11)) and experimental results for the mean quadratic velocity; (Middle part) Results of the proposed procedure for five different draws of the wall-pressure field on the 0 – 1000 Hz frequency range; (Lower part) Results of the proposed procedure for five different draws of the wall-pressure field on the 100 – 300 Hz frequency range.

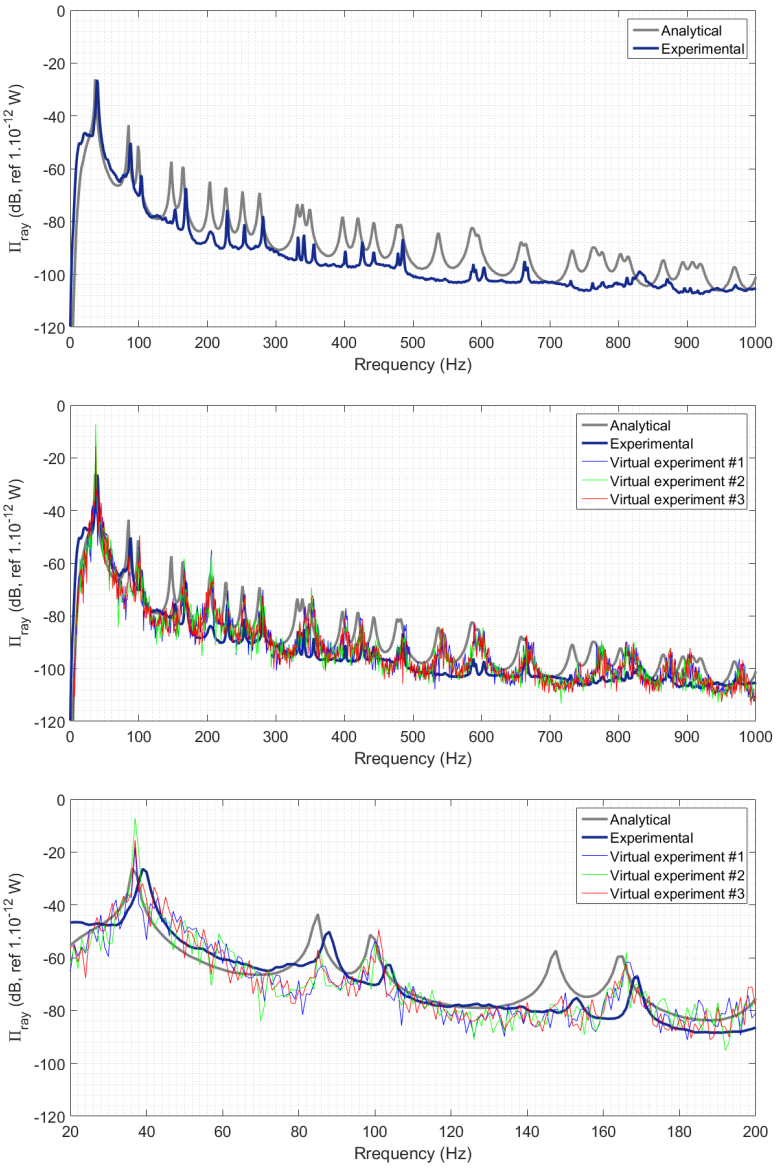

Fig. 7 (Upper part) Analytical calculations (Eq. (14)) and experimental results for the radiated sound power; (Middle part) Results of the proposed procedure for three different draws of the wall-pressure field on the 0 – 1000 Hz frequency range; (Lower part) Results of the proposed procedure for three different draws of the wall-pressure field on the 20 – 200 Hz frequency range.

an inverse short-time Fourier transform can be used to recover a signal of varying length (provided that the constant overlap-add constraint is followed [51, 52]).

The synthesized sound pressure was in this case obtained using the inverse Fourier transform of four successive draws (leading to a signal of 4 seconds with a sampling frequency of 2048 Hz). The measured and calculated sound pressure as a function of time are shown in Fig. 8 on a zoomed time scale (over a second). The amplitude of the measured signal as well as its variations as a function of time are well captured. Note that no phase alignment was performed in this case. In other words, the starting point for each signal is arbitrary.

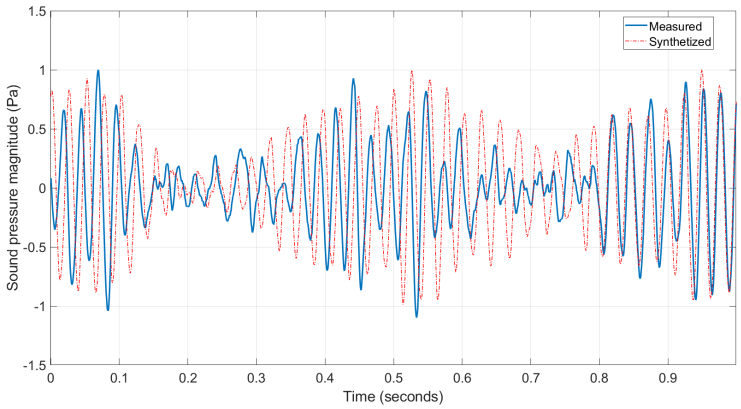

Fig. 8 Comparison of the measured sound pressure level at the considered microphone position (continuous line) and the synthesized sound pressure level at the same position (dashed line).

6 Conclusion

A method based on spectral synthesis was proposed for generating space-time wall pressure fields for random excitations like DAF or TBL. In this work, this approach was coupled to an analytical model of a simply-supported panel and was used to predict its vibracoustic behavior under a low-speed TBL excitation. It was shown that it could be used to perform virtual experiments on plane structures, these virtual experiments corresponding to consecutive realizations of the wall-pressure field.

Based on this first proof-of-concept, a first perspective consists in coupling the synthesis approach with FEM models in order to apply it to complex structures like stiffened panels, and directly obtain the radiated sound pressure as a function of time.

Another perspective lies in the use of these virtual experiments realizations to study dispersion in actual laboratory measurements under random excitations, and

to identify main sources of data scattering as in coupled rooms [53] and wind-tunnel measurements.

Acknowledgements This work was performed within the framework of the Labex CeLyA of "Université de Lyon" (ANR-10-LABX-0060/ ANR-11-IDEX-0007) and of the VIRTECH project (ANR-17-CE10-0012), operated by the French National Research Agency. The support of "Laboratoire International Associé - Centre d'Acoustique Jacques Cartier" (supported by the French National Research Agency) is also acknowledged. Finally, the authors thank Pierre Chainais for his fruitful suggestions that rooted this work.

References

1. E. Ciappi, S. De Rosa, F. Franco, J.-L. Guyader, and S.A. Hambric (Eds.), 'Flinovia - Flow Induced Noise and Vibration Issues and Aspects - A Focus on Measurement, Modeling, Simulation and Reproduction of the Flow Excitation and Flow Induced Response', Springer, 358 pages (2015).
2. E. Ciappi, S. De Rosa, F. Franco, J.-L. Guyader, S.A. Hambric, R.C.K. Leung, A. D. Hanford (Eds.), 'Flinovia - Flow Induced Noise and Vibration Issues and Aspects II - A Focus on Measurement, Modeling, Simulation and Reproduction of the Flow Excitation and Flow Induced Response', Springer, 372 pages (2017).
3. G.R. Ludwig, An experimental investigation of the sound generated by thin steel panels excited by turbulent flow (boundary layer noise), UTIA report NO. 87 (1962).
4. L. Maestrello, Measurement of noise radiated by boundary layer excited panels", Journal of Sound and Vibration, 2 (2), 100-115 (1965).
5. D.A. Bies, A review of flight and wind tunnel measurements of boundary layer pressure fluctuations and induced structural response, NASA CR626, 96 pages (1966).
6. H.G. Davies, Sound from Turbulent-Boundary-Layer-Excited Panels, The Journal of the Acoustical Society of America 49:3B, 878-889 (1969).
7. G.M. Corcos, Resolution of Pressure in Turbulence, J. Acoust. Soc. Am. 35, 192-199 (1963).
8. M. Bull. Wall-pressure fluctuations associated with subsonic turbulent boundary layer flow. Journal of Fluid Mechanics, 28(4), 719-754 (1967).
9. N. Hu, C. Appel, S. Haxter, S. Callsen and A. Klabes. Simulation of wall pressure fluctuations on Airbus-A320 fuselage in cruise flight condition, 25th AIAA/CEAS Aeroacoustics Conference, Delft, The Netherlands, 20-23 May 2019.
10. S. L. Prigent, É. Salze and C. Bailly. Deconvolution of Wave-Number-Frequency Spectra of Wall Pressure Fluctuations, AIAA Journal 58:1, 164-173 (2020).
11. Y.M. Chang and P. Leehey, "Vibration of and acoustic radiation from a panel excited by adverse pressure gradient flow", MIT report No. 70208-12, 1-33 (1976).
12. M. Smith and E. Latorre Iglesias, "Vibration and noise radiation from a panel excited by a turbulent flow", in Proc. Acoustics2012, Société Française d'Acoustique, Nantes, France 2012, 1845-1850.
13. B. Liu, H. Zhang, Z. Qian, D. Chang, Q. Yan and W. Huang, "Influence of stiffeners on plate vibration and radiated noise excited by turbulent boundary layers", Applied Acoustics, 80, 28-35, (2014).
14. J. Osterziel, F.J. Zenger and S. Becker, "Sound radiation of aerodynamically excited flat plates into cavities", Applied Sciences 7, 1062, 2017.
15. N. Oettle and D. Sims-Williams, Automotive aeroacoustics: An overview. Proceedings of the Institution of Mechanical Engineers, Part D: Journal of Automobile Engineering, 231(9), 1177–1189 (2017).
16. M.K. Bull. Wall-pressure fluctuations beneath turbulent boundary layers: some reflections on forty years of research, Journal of Sound and Vibration, 190(3), 299-315 (1996).

17. T. Bravo and C. Maury. The experimental synthesis of random pressure fields: Methodology. The Journal of the Acoustical Society of America 120, 2702 (2006).
18. N.B. Roozen, Q. Leclère, D. Urbán, L. Kritly, C. Glorieux. Assessment of the sound reduction index of building elements by near field excitation through an array of loudspeakers and structural response measurements by laser Doppler vibrometry. Applied Acoustics 140, 225-235 (2018).
19. O. Kirkeby and P. A. Nelson, Reproduction of plane wave sound fields, J. Acoust. Soc. Am. 94(5), 2992–3000 (1993).
20. T. Bravo and C. Maury, A synthesis approach for reproducing the response of aircraft panels to a turbulent boundary layer excitation. Journal of the Acoustical Society of America Vol. 129(1), pp. 143-153 (2011).
21. C. Maury and T. Bravo, Laboratory synthesis of the response of aircraft panels to a turbulent boundary layer excitation (Invited contribution in Aeroacoustics research in Europe : The CEAS-ASC report on 2010 highlights), J. Sound Vib., 330, 4970-4971 (2011).
22. M. Aucejo, L. Maxit and J.-L. Guyader, Experimental simulation of turbulent boundary layer induced vibrations by using a synthetic array, J Sound Vib 331 (16), 3824–3843 (2012).
23. O. Robin, A. Berry and S. Moreau, Experimental vibroacoustic testing of plane panels using synthesized random pressure fields, J. Acoust. Soc. Am. 135, 3434 (2014).
24. C.A. Merlo, A.M. Pasqual and E.B. Medeiros, Sound field synthesis on flat panels using a planar source array controlled by its active and reactive radiation modes, Acta Acustica United Ac. 105, 139-151 (2019).
25. A.M. Pasqual, Analysis of the complex sound power in the near field of spherical loudspeaker arrays, J. Sound Vib., 456, 331-352 (2019).
26. C. Marchetto, L. Maxit, O. Robin, A. Berry. Experimental prediction of the vibration response of panels under a turbulent boundary layer excitation from sensitivity functions. The Journal of the Acoustical Society of America 143:5, 2954-2964, (2018).
27. C.S. Wolowicz, J.S. Bowman, and W.P. Gilbert. Similitude Requirements and Scaling Relationships as Applied to Model Testing. NASA Technical paper 1435 (1979).
28. A. Casaburo, G. Petrone, F. Franco, S. De Rosa. A Review of Similitude Methods for Structural Engineering. ASME. Appl. Mech. Rev. May 71(3): 030802 (2019).
29. X. Zhao and B. Ai. Predicting the Structural Response Induced by Turbulent Boundary Layer in Wind Tunnel. AIAA Journal 55:4, 1221-1229 (2017).
30. F. Franco, O. Robin, E. Ciappi, S. De Rosa, A. Berry, G. Petrone. Similitude laws for the structural response of flat plates under a turbulent boundary layer excitation. Mechanical Systems and Signal Processing, 129, 590-613 (2019).
31. H. Yao and L. Davidson, Vibro-acoustics response of a simplified glass window excited by the turbulent wake of a quarter-spherocylinder body, The Journal of the Acoustical Society of America 145:5, 3163-3176 (2019).
32. P. Druault, A. Hekmati and D. Ricot, Discrimination of acoustic and turbulent components from aeroacoustic wall pressure field, Journal of Sound and Vibration, 32 (26), 7257-7278 (2013).
33. Hu N., Reiche N., and Ewert, R. Simulation of turbulent boundary layer wall pressure fluctuations via Poisson equation and synthetic turbulence. Journal of Fluid Mechanics, 826, 421-454 (2017).
34. C. Hong and K.-K. Shin, Modeling of wall pressure fluctuations for finite element structural analysis, Journal of Sound and Vibration, 329 (10), (2010).
35. A. Hekmati, D. Ricot, and P. Druault, Numerical synthesis of aeroacoustic wall pressure fields over a flat plate: Generation, transmission and radiation analyses, Journal of Sound and Vibration 332(13):3163–3176 (2013) DOI: 10.1016/j.jsv.2013.01.019
36. M. Karimi, P. Croaker, H. Peters, S. Marburg, A. Skvortsov and N. Kessissoglou, Vibro-acoustic response of a flat plate under turbulent boundary layer excitation, Proceedings of NOVEM 2018 – Noise and Vibration Emerging Methods; Ibiza, Spain (2018).
37. M. Karimi, P. Croaker, L. Maxit, O. Robin, A. Skvortsov, S. Marburg and N. Kessissoglou, A hybrid numerical approach to predict the vibrational responses of panels excited by a turbulent boundary layer, Journal of Fluids and Structures, 92, 102814 (2020).

38. L. Maxit, Simulation of the pressure field beneath a turbulent boundary layer using realizations of uncorrelated wall plane waves, The Journal of the Acoustical Society of America 140, 1268 (2016).
39. O. Robin, M. Pachebat, N. Totaro and A. Berry, Évaluation d'une méthode de synthèse spectrale 2D+T pour la transparence de parois sous champ acoustique diffus. CFA / VISHNO 2016, Apr 2016, Le Mans, France.
40. M. Jenzri, O. Robin and N. Atalla, Vibration of and radiated acoustic power from a simply-supported panel excited by a turbulent boundary layer excitation at low Mach number. Noise Control Engineering Journal, 67(4), 241-251 (2019).
41. G.J.M. Aitken, Long and short-term correlation properties of computer-generated fractional Gaussian noise. Physica A: Statistical Mechanics and its Applications, 333, 1-9 (2004).
42. R.B. Davies and D.S. Harte, Tests for Hurst effect. Biometrika, 74(1), 95–101 (1987).
43. A. Papoulis and U. Pillai, Probability, random variables and stochastic processes. McGraw-Hill Higher Education, 515-519 (2002).
44. X. Gloerfelt and J. Berland, Direct Computation of Turbulent Boundary Layer Noise, proceedings of the 15th AIAA/CEAS Aeroacoustics Conference (30th AIAA Aeroacoustics Conference), American Institute of Aeronautics and Astronautics, may 2009.
45. L.E. Wittig and A.K. Sinha, Simulation of multicorrelated random processes using the FFT algorithm J. Acoust. Soc. Am. 58, 630-634 (1975).
46. R.H. Mellen, Wave-vector filter analysis of turbulent flow The Journal of the Acoustical Society of America 95, 1671-1673 (1994).
47. G. Schewe, On the Structure and Resolution of Wall-Pressure Fluctuations Associated with Turbulent Boundary-Layer Flow Journal of Fluid Mechanics, 134, 311-328 (1983).
48. O. Robin, J.-D. Chazot, R. Boulandet, M. Michau, A. Berry, N. Atalla. A plane and thin panel with representative simply supported boundary conditions for laboratory vibroacoustic tests Acta Acust. United Acust., 102 (1), 170-182 (2016).
49. O. Robin, S. Moreau, T. Padois and A. Berry. Measurement of the wavenumber-frequency spectrum of wall pressure fluctuations: Spiral-shaped rotative arrays with pinhole-mounted quarter inch microphones, in proceedings of the 19th AIAA/CEAS Aeroacoustics Conference, Berlin, Germany (2013).
50. ISO 3744:2015, "Acoustics – Determination of sound power levels and sound energy levels of noise sources using sound pressure – Engineering methods for an essentially free field over a reflecting plane". International Organization for Standardization, Geneva, Switzerland.
51. R.E. Crochiere. A Weighted Overlap-Add Method of Short-Time Fourier Analysis/Synthesis, IEEE Transactions on Acoustics, Speech and Signal Processing. Vol. 28, No. 1, Feb 1980, pp. 99–102 (1980).
52. J.O. Smith. Spectral Audio Signal Processing. https://ccrma.stanford.edu/ jos/sasp/, online book, 2011 edition, accessed Dec 2019.
53. A. Dijckmans, G. Vermeir. Numerical investigation of the repeatability and reproducibility of laboratory sound insulation measurements, Acta Acustica united with Acustica 99 (3), 421-432 (2013)